Thicker clouds and accelerated Arctic sea ice decline: Atmosphere-sea ice interactions in Spring

Yiyi Huang[1]

David A. Bailey[2], Marika M. Holland[2], Xiquan Dong[1], Baike Xi[1]

Alice K. DuVivier[2], Jennifer Kay[3], Laura Landrum[2], Yi Deng[4]

[1]University of Arizona, Tucson, AZ

[2]National Center for Atmospheric Research, Boulder, CO

[3]University of Colorado Boulder, Boulder, CO

[4]Georgia Institute of Technology, Atlanta, GA

February 4, 2019

Motivation

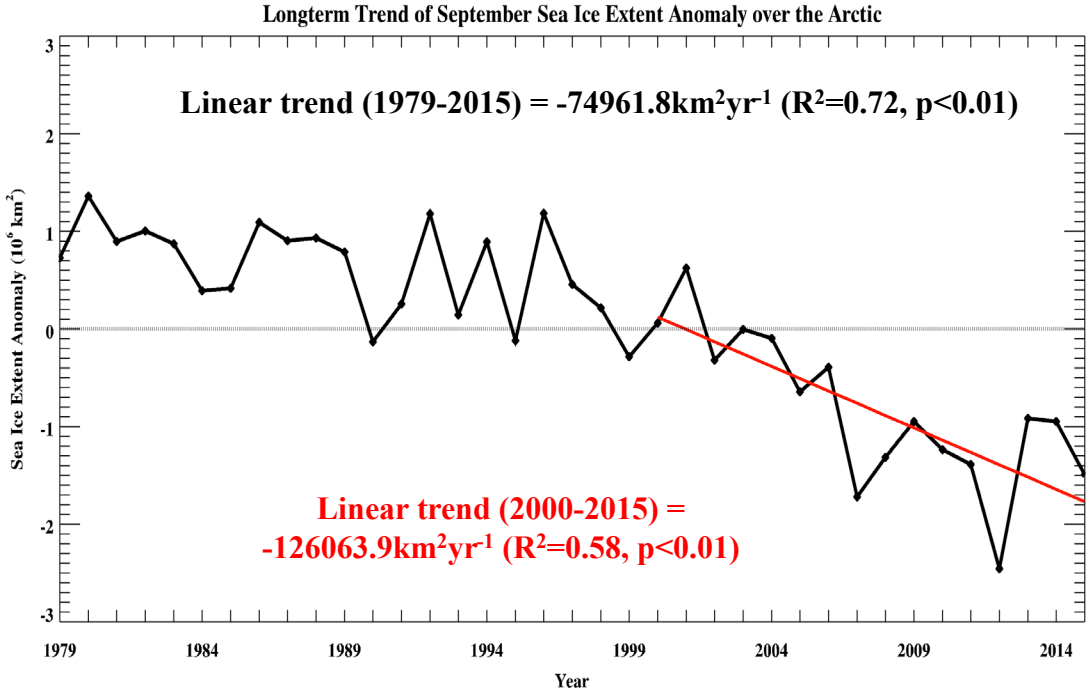

- The changes in sea ice over the Arctic are caused by different dynamic and thermodynamic forces
- Among them, cloud and surface energy budget anomalies were found to be important drivers for observed trends and variability in Arctic sea ice

Shrinking Arctic Sea Ice Cover and Increasing Springtime Clouds In Early 21st Century (2000-2015)

Sept. Sea Ice Trend

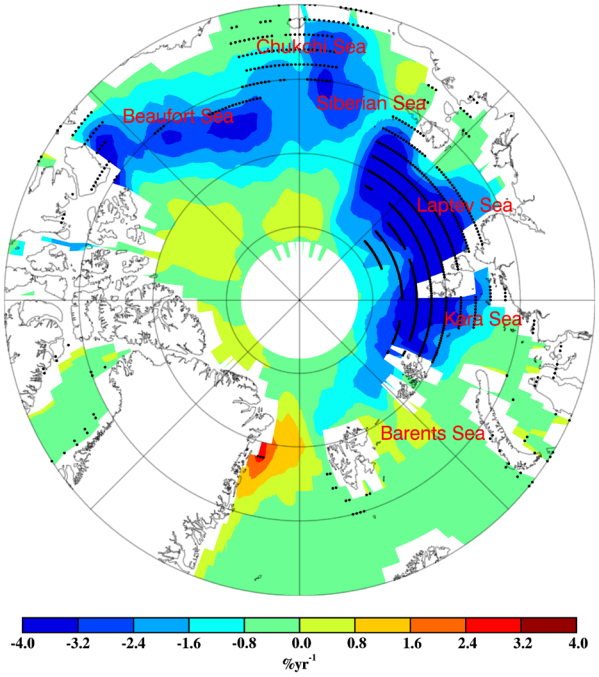

Huang et al. (2017a), *JGR*

**Black dots mark 95% significance level*

- September sea ice concentration has been retreating rapidly over the Siberian Sea, Laptev Sea and Kara Sea during the period of 2000-2015
- There are significant positive cloud fraction linear trends in spring from NASA CERES-MODIS satellite retrievals, especially from March to May

Cloud Fraction Trend

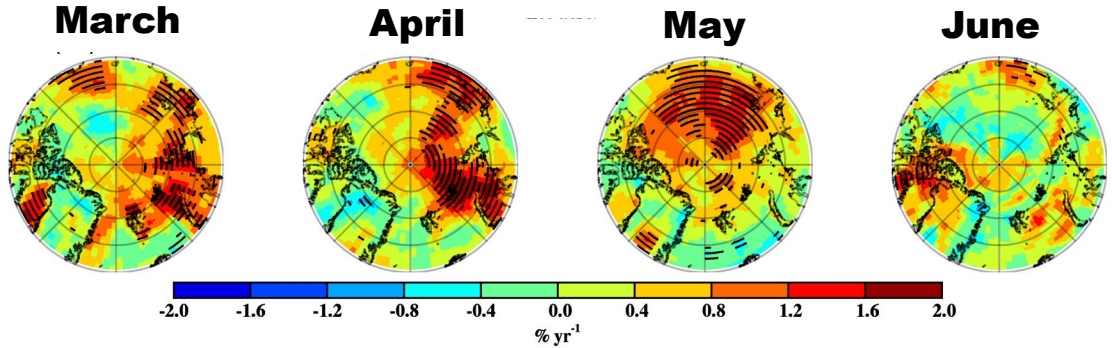

Data

➢ **Model simulation: CESM Large Ensemble (CESM-LE)**

The CESM-LE is run with fully coupled atmosphere, ocean, land and sea ice components from 1920 to 2100. Using the same model and external forcing, but with small round-off level variations in their sea surface temperature initial conditions, the CESM-LE project provides a comprehensive resource for studying climate change in the presence of internal climate variability.

➢ **Satellite retrievals (cloud properties): NASA CERES-MODIS SYN1 Edition 3A**

Cloud properties including CF and CWP used in this study are from the Clouds and Earth's Radiant Energy System (CERES) Moderate Resolution Imaging Spectroradiometer (MODIS) SYN1 Edition 3A monthly gridded dataset (1° × 1°) from March 2000 to February 2017, which is derived from both Aqua and Terra satellite measurements

➢ **Satellite retrievals (radiative properties): NASA CERES EBAF-Surface Edition 2.8**

The surface radiation fluxes are from CERES Energy Balanced And Filled (EBAF)-Surface Edition 2.8 datasets, with monthly temporal scale and 1° × 1° spatial resolution.

➢ **Satellite retrievals (sea ice): Nimbus-7 sea ice concentration**

Daily SIC is obtained from Nimbus-7 SSMR and DMSP SSM/I-SSMIS passive microwave data version-1 provided by the National Snow and Ice Data Center. SIC is derived from surface brightness temperatures measured from the following sensors: Nimbus-7 SMMR, the DMSP-F8, -F11 and -F13 SSM/I, and the DMSP-F17 SSMIS. The data is provided in the polar stereographic projection with a grid cell size of 25 km × 25 km in polar stereographic grid from October 1978 to present.

The CF trend in April during 2006-2021

- The CF linear trends differ considerably across 40 members in the CESM-LE
- Their spread cloud fraction linear trends can be attributed to internally generated climate variability alone

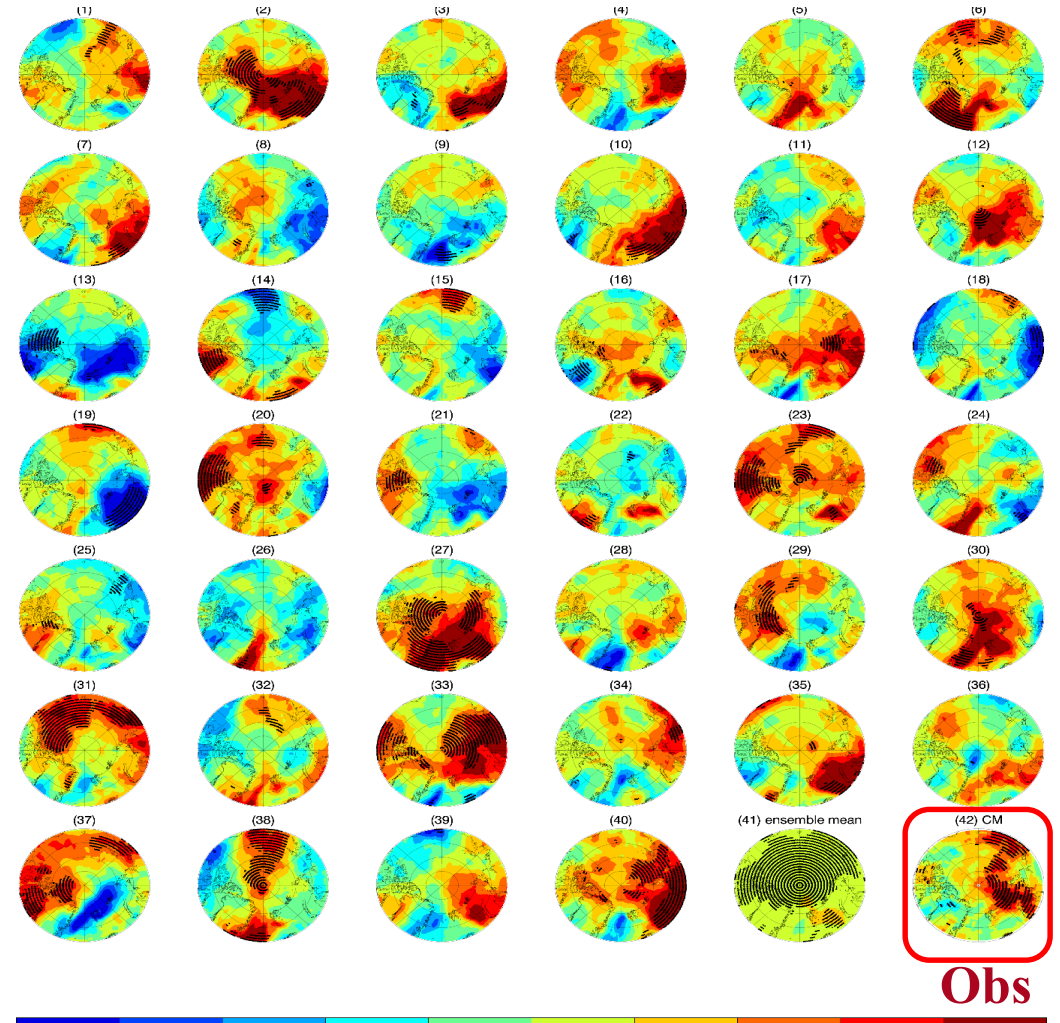

*Black dots mark 95% significance level

Relationships between September sea ice minimum with springtime cloud and radiation properties

- The simulated September sea ice changes tend to be more sensitive to cloud water path than cloud fraction in the model
- Cloud longwave effect on the sea ice melting increases from March to June in CESM-LE on a seasonal basis

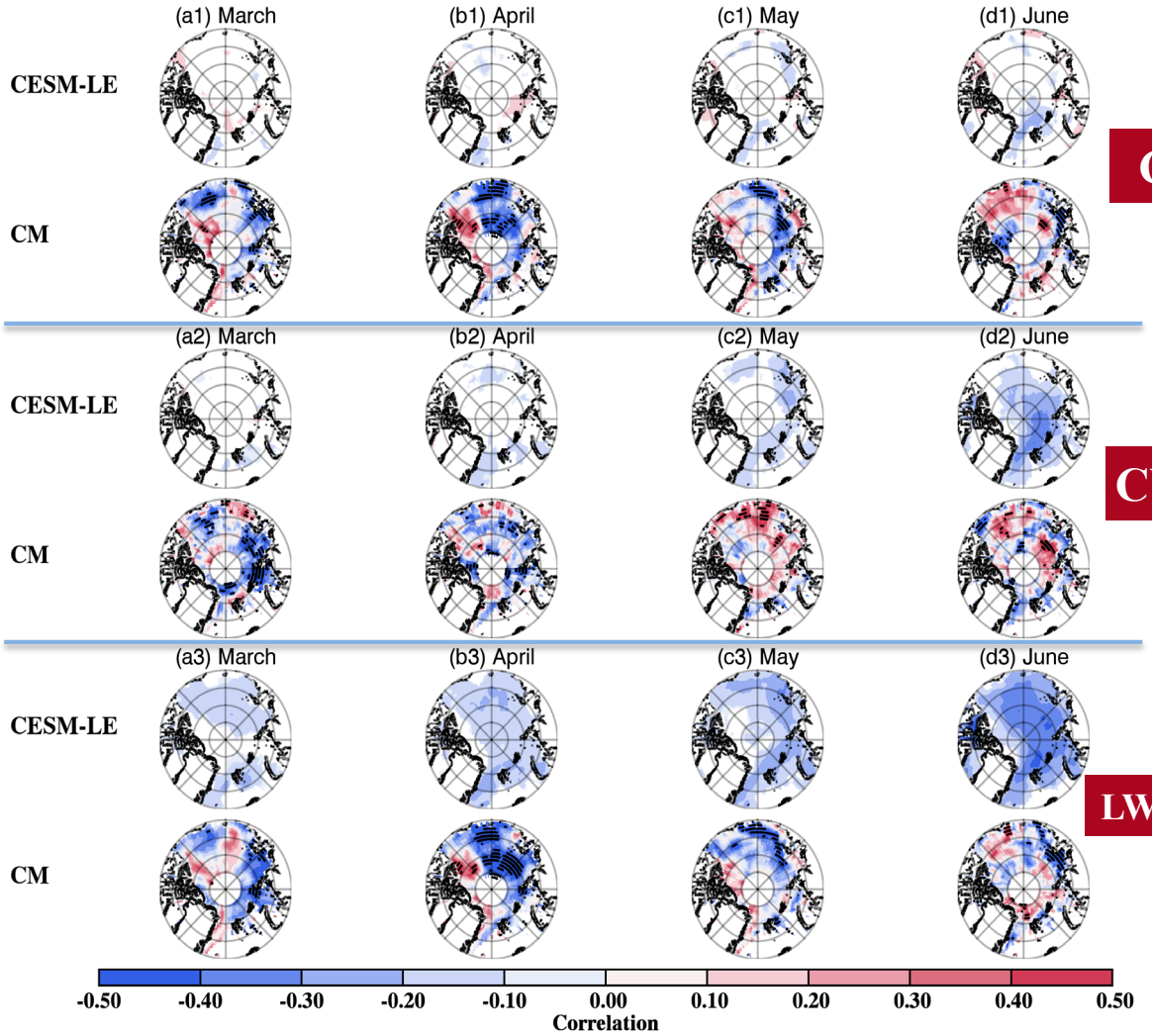

*Black dots mark 95% significance level

CESM AMIP Experimental Design

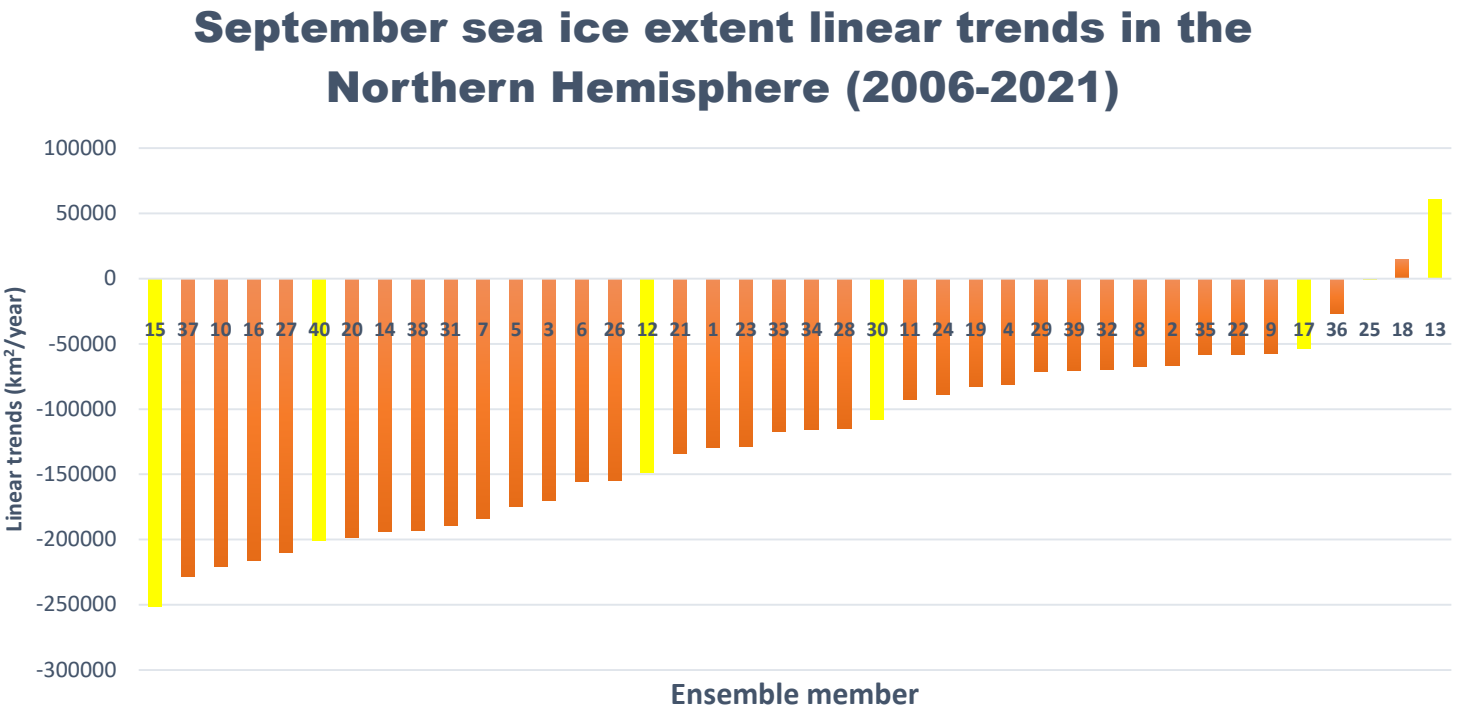

- To investigate atmospheric response under different Arctic sea ice trends

CESM AMIP Experimental Design

- We use different values of SST, sea ice concentration and sea ice thickness in the sea ice covered regions in the Northern Hemisphere and 40-member ensemble mean in the tropics and Southern Hemisphere

Model Configuration

Model version: CESM1_2_2_1

Resolution: f09_g16

Atmosphere/Land: 0.9x1.25
Ice/Ocean: gx1v6 (displaced pole)

Compset: FAMIPC5

Active atmosphere (CAM5)/land, prescribed sea ice/SST and data ocean

Time period: 2006-2021

Temporal resolution: Monthly

External forcing: RCP8.5

The regression slope between September sea ice extent in Northern Hemisphere and sea ice thickness for summer and winter (July-December)

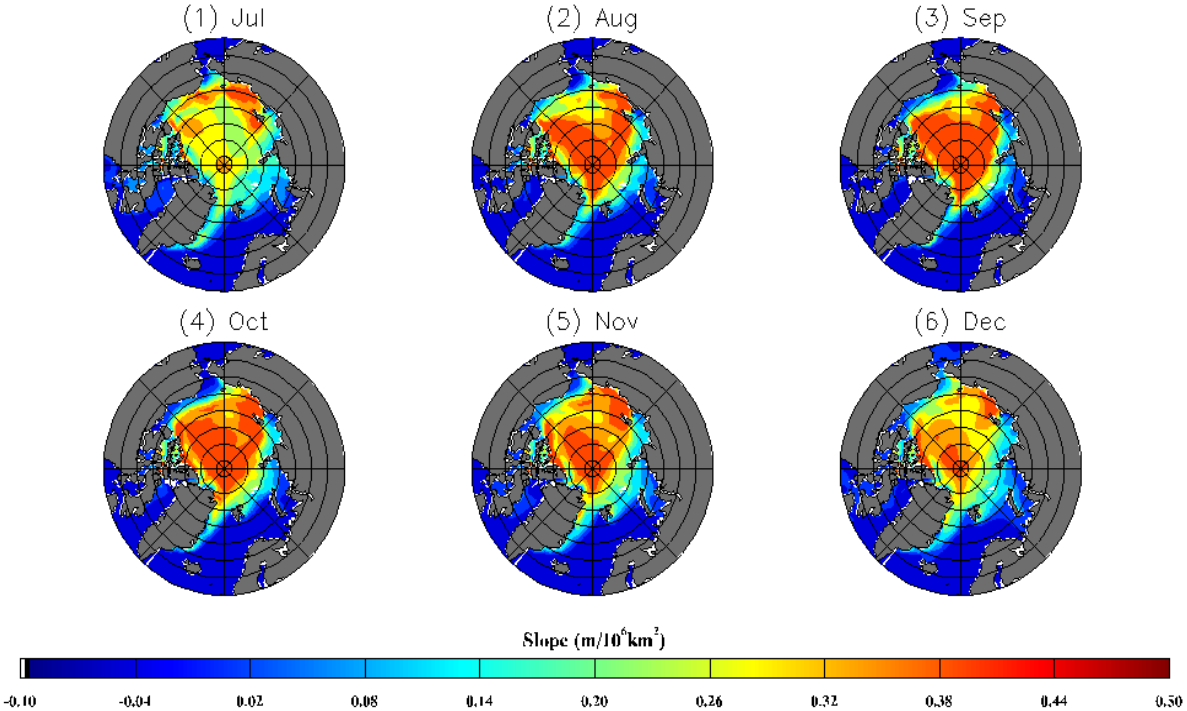

The linear trends of Arctic SIC, cloud and radiation properties for March during 2006-2021 in CESM AMIP experiments

- With accelerated sea ice decline and surface warming, the springtime presence of more open water generates stronger evaporation, which favors the formation of clouds

- The result is a positive feedback where more clouds lead to increased downward longwave flux, which further enhances sea ice melt

**Black dots mark 95% significance level*

SIC

SST

EVPR

LWP

LW_down

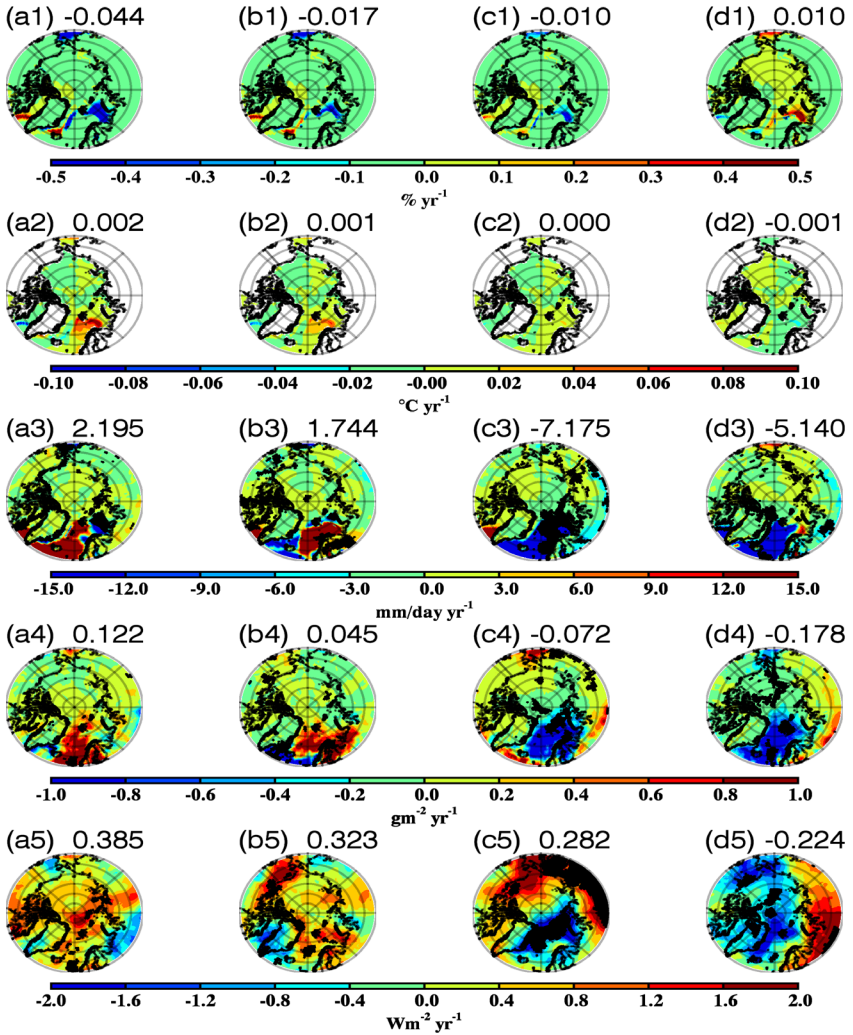

The linear trends of springtime total cloud water path (liquid + ice) in CESM AMIP experiments during the period 2006-2021

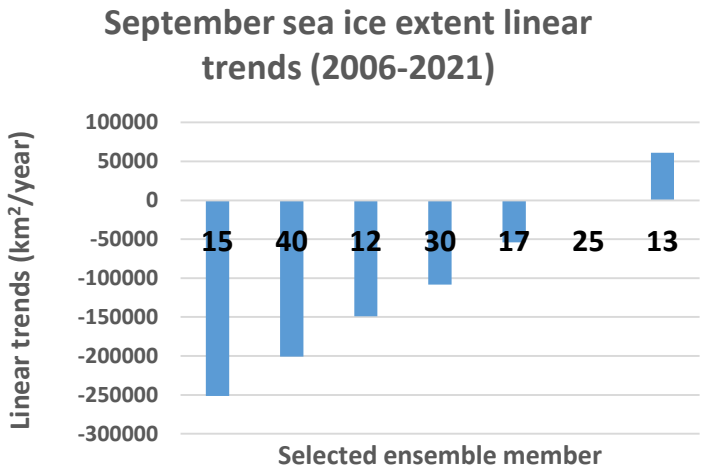

- The cloud response to sea ice loss largely depends on the strength of atmosphere-ocean coupling which is modulated by air-sea temperature gradients and near-surface static stability in the Arctic

**Black dots mark 95% significance level*

March

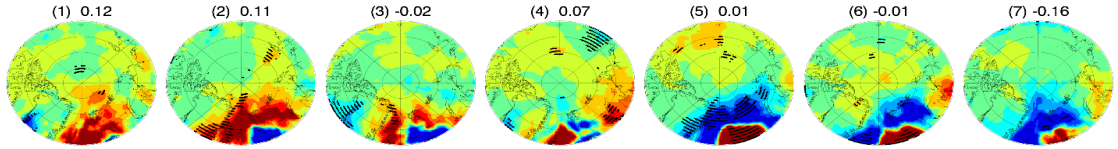

April

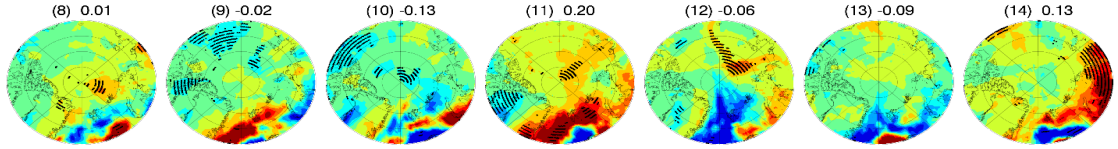

May

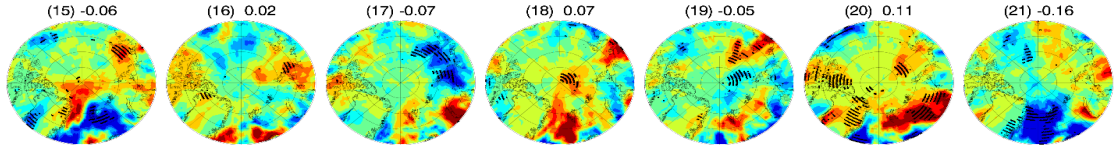

June

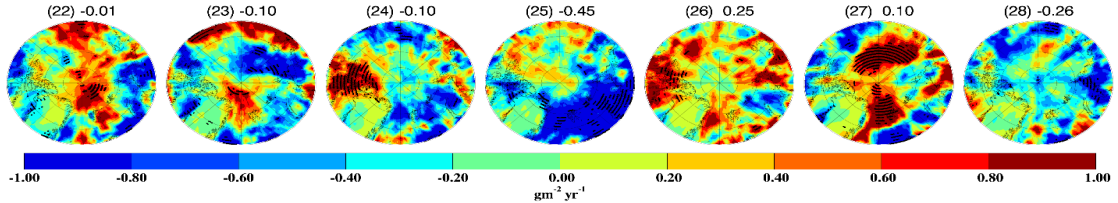

The Schematic Diagram about Feedback Mechanisms

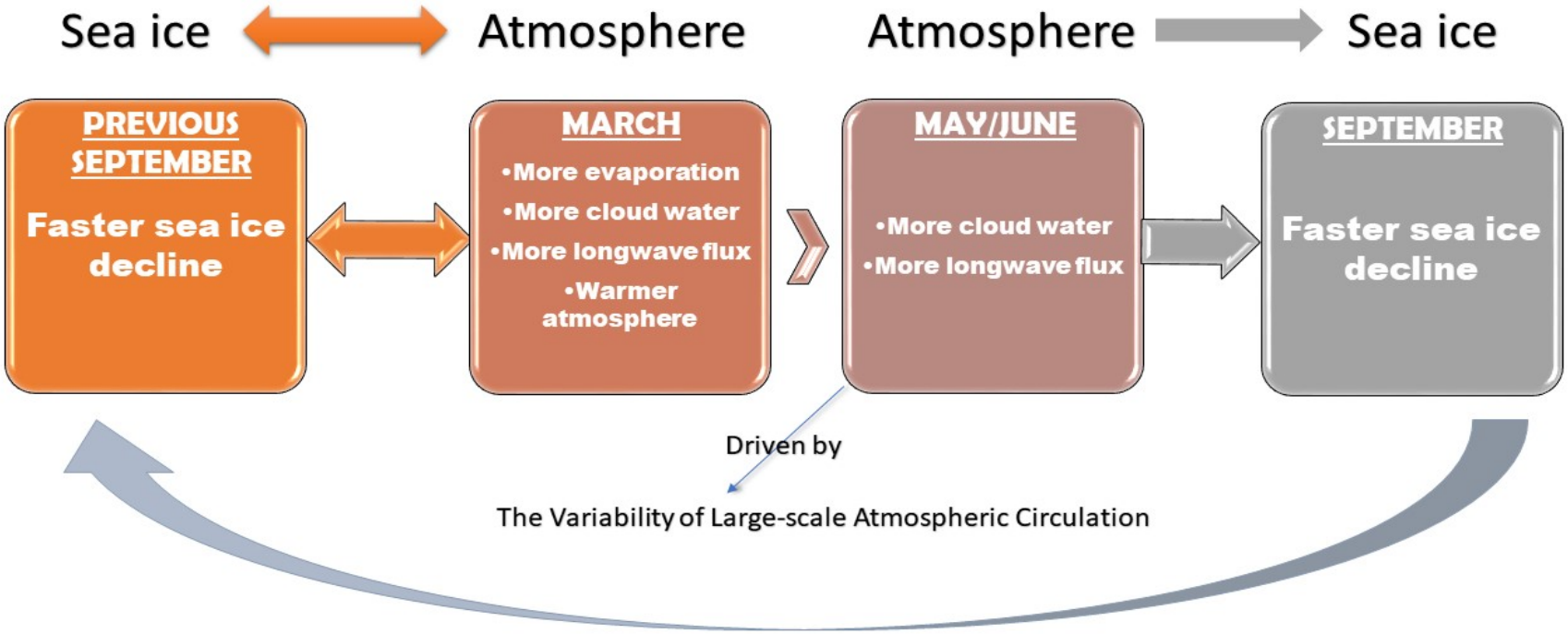


THE UNIVERSITY
OF ARIZONA

The difference of linear trends of total cloud water path (liquid + ice) between CESM AMIP simulations and CESM-LE results during the period 2006-2021

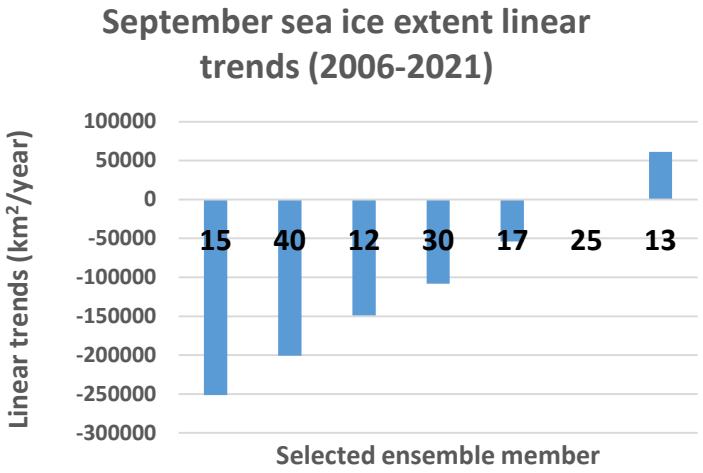

*Only the difference of two datasets with 95% statistically significance level is shown in each panel

March

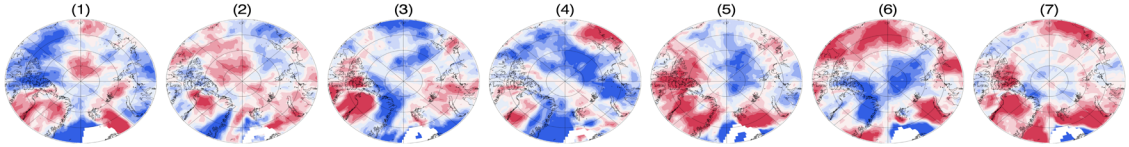

April

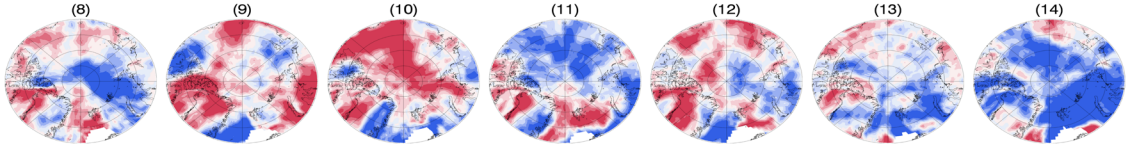

May

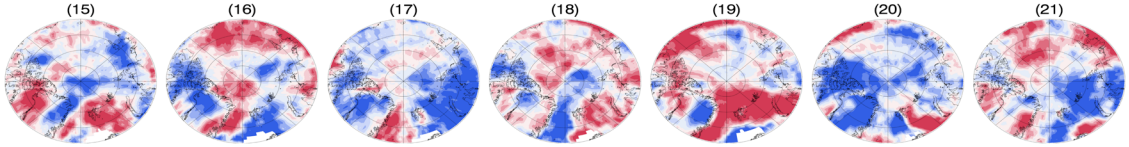

June

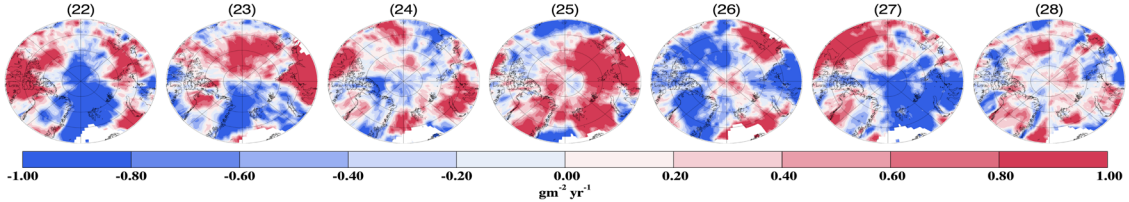

Cloud and radiation linear trends (2000-2015)

CF

CWP

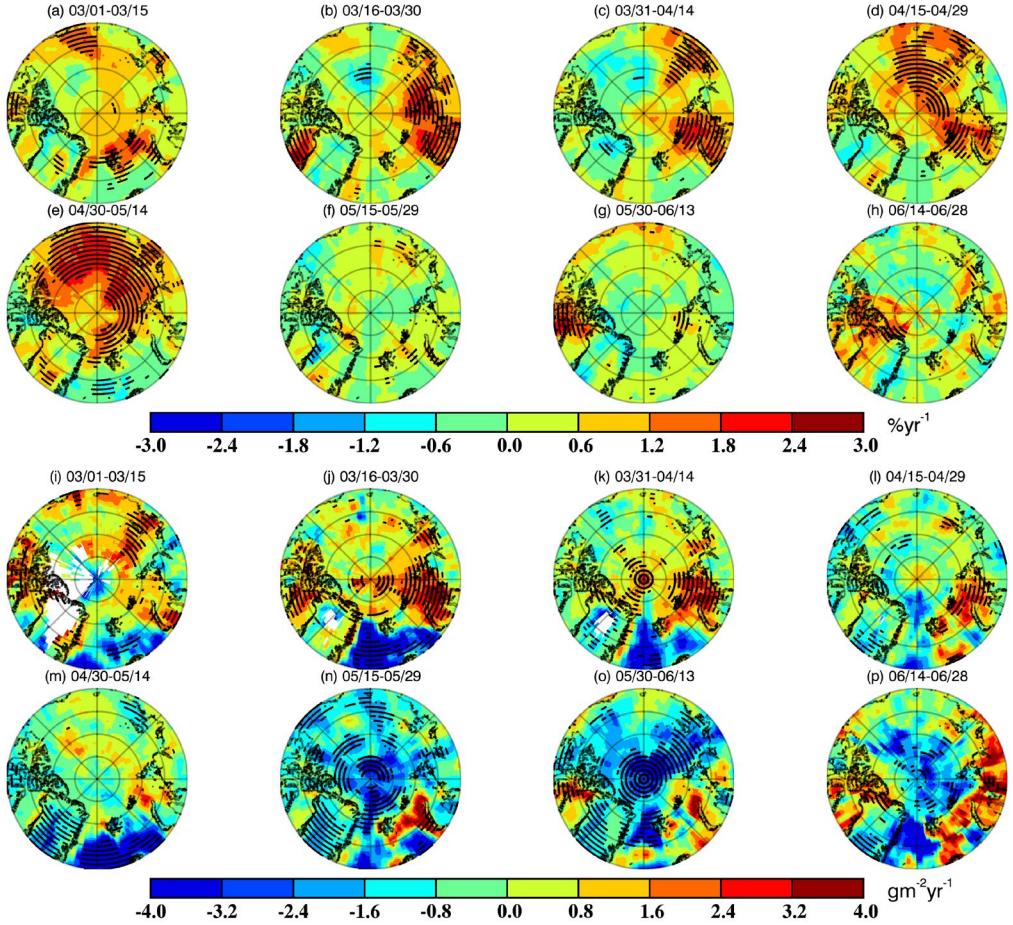

Cloud and radiation linear trends (2000-2015)

LW_down

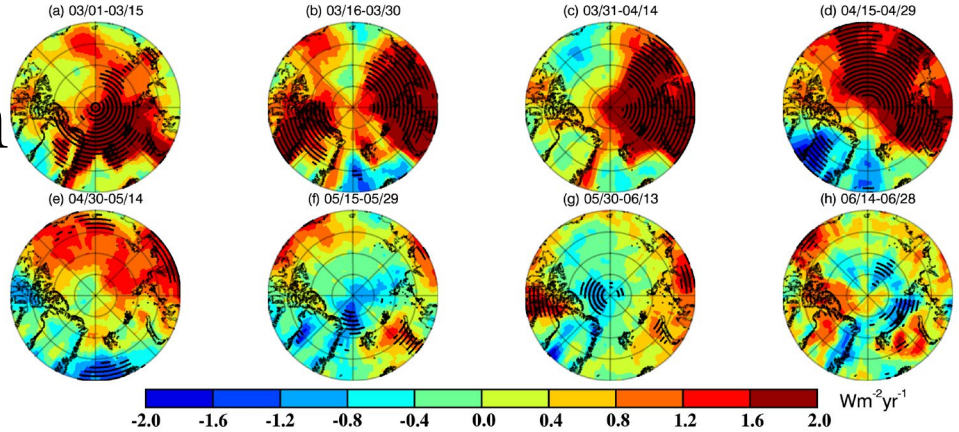

SW_down

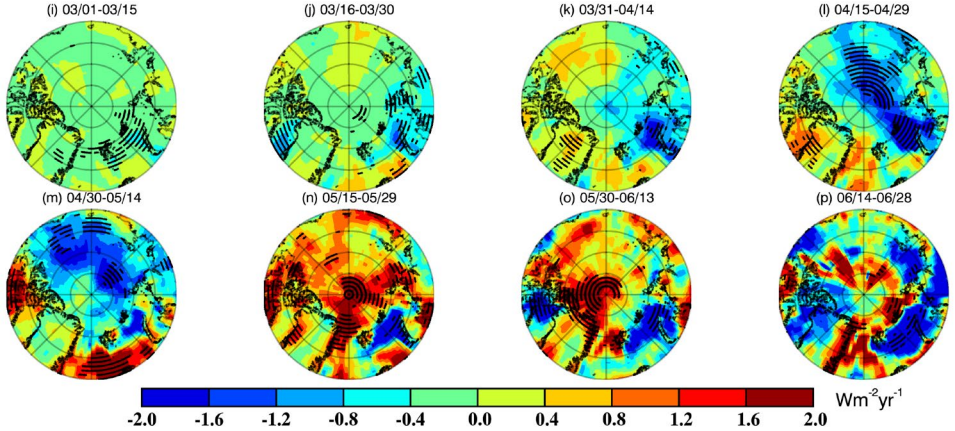

Backup: CM uncertainties

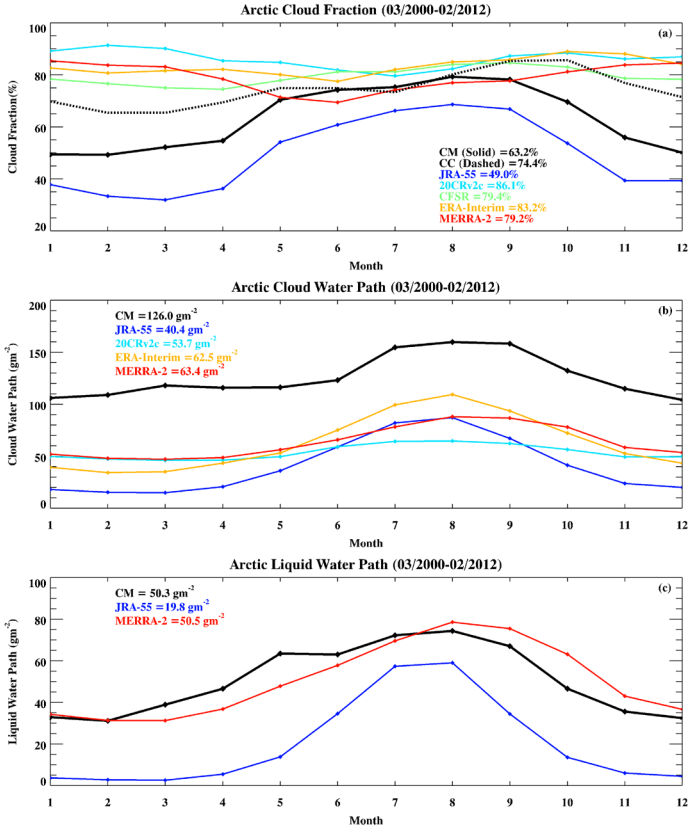

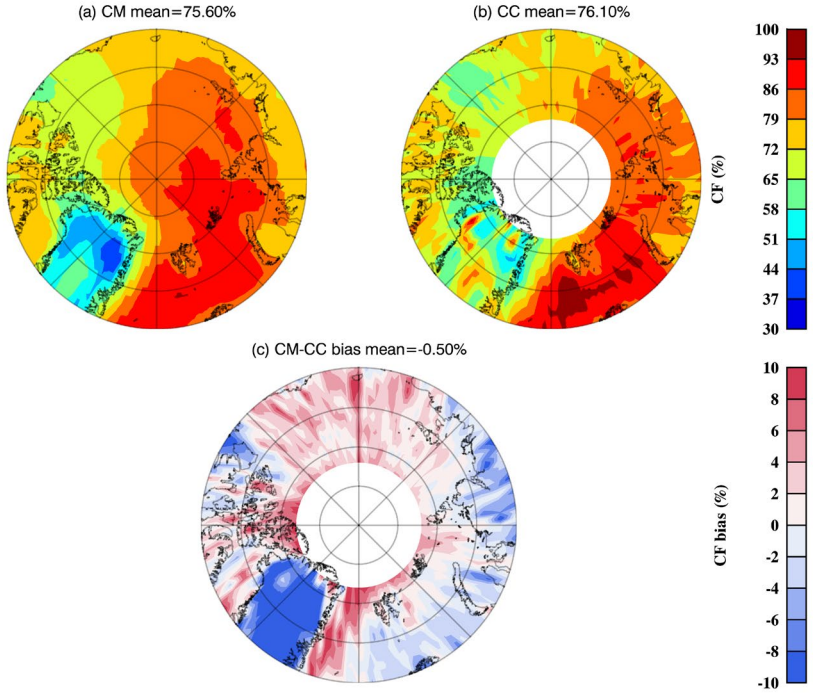

Backup: CM uncertainties

Table 1 Seasonal and annual biases and RMSDs (in parentheses) of CM derived surface radiative fluxes against the surface observations (averages from BAR, NYA, ALE, GRS and HMB) within the Arctic (70°-90°N)

	Surface SW_down flux (Wm^{-2})	Surface LW_down flux (Wm^{-2})
DJF	+0.12 (1.58)	+6.46 (6.47)
MAM	−1.34 (2.35)	+8.94 (9.76)
JJA	+8.86 (9.06)	+0.88 (2.05)
SON	+1.42 (2.94)	+1.35 (3.33)
Annual	+2.27 (4.91)	+4.41 (6.17)

Cloud-radiation relationships in SFC observations

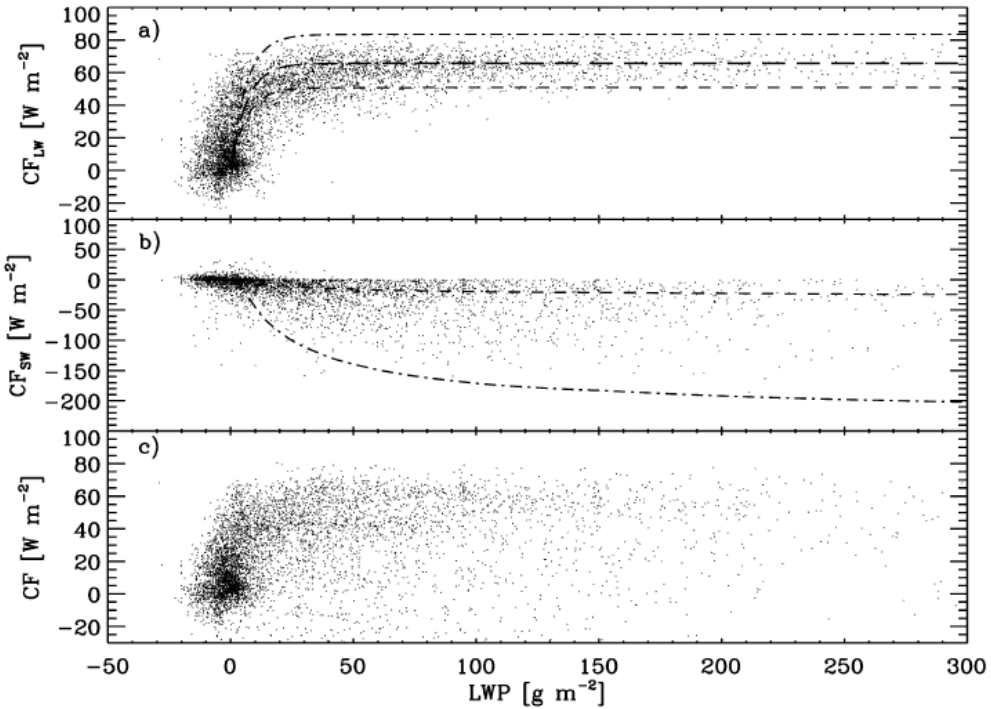

FIG. 6. Observed relationship between MWR-derived LWP and (a) CF_{LW}, (b) CF_{SW}, and (c) CF. Curves in (a) are derived from Eq. (3) using typical cloud temperatures of 0° (dash–dot), −20° (long dash), and −40°C (short dash). Cloud base and LW atmospheric transmittance were assumed to be 1 km and 0.9, respectively. Curves in (b) are derived from Eq. (5) for typical spring (short dash) and midsummer (dash–dot) conditions using values for θ, α_s of 80°, 0.8 and 60°, 0.5 respectively.

SHEBA field campaign (Oct.1997-Oct.1998, Beaufort and Chuckchi Seas north of Alaska)

- The CF_{LW} increases with LWP until LWP =30 g m^{-2}, after which point clouds emit as blackbodies, and increasing LWP has no further impact on downwelling LW radiation
- The changes in LWP are most important in high, optically thin yet relatively warm clouds, such as the frequent Arctic winter mixed-phase clouds
- The magnitude of CF_{sw} typically increases with LWP and cloud scenes with little LWP have only a small cooling effect
- The sensitivity of CF_{sw} to cloud microphysics is particularly important for thick clouds
- As LWP increases, the cloud SW shading effect continues to increase after the LW greenhouse effect becomes saturated

Shupe and Intrieri (2004), *J. Climate*

Monthly means of liquid water path over the Arctic